Timing of the anthropogenic carbon invasion in the Southern California Current

Yéssica Vanessa Contreras-Pacheco[1,3], Jose Luis Abella Gutiérrez[1,2], Gerardo Vallejo Espinosa[1,3] and Juan Carlos Herguera García[1]*

[1]Division of Oceanography, Center for Scientific Research and Higher Education of Ensenada (CICESE), Ensenada, Mexico

[2] Jackson School of Geosciences, The University of Texas at Austin, Austin, TX, USA

[3]Materials, Water and Energy Research Laboratory, Department of Engineering, University of Guadalajara (UdeG), Tepatitlán de Morelos, Mexico

Corresponding author: *Juan Carlos Herguera (herguera@cicese.mx)

Abstract

The Eastern Boundary Upwelling Systems (EBUS), such as the Southern California Current System (CCS), are well-known high-productivity regions driven by alongshore winds, although their role as oceanic sources and sinks of atmospheric CO_2 in the global carbon cycle is poorly understood. In the southern CCS, off Baja California, wind-driven vertical mixing upwells nutrient and carbon-rich waters from late winter to early summer, while weaker winds during the rest of the year allow the intrusion of nutrients and carbon-depleted subtropical surface waters. Here, we interpret the isotopic composition of organic carbon and calcitic records spanning ~160 years from high-resolution sediment cores collected off Baja California, showing a clear trend toward lighter carbon isotopic compositions of the organic and inorganic carbon for the past seven decades. These trends are similar to the atmospheric records associated with the ^{13}C Suess effect, suggesting an atmospheric carbon invasion into the surface waters of the California Current. Nevertheless, the slope of the atmospheric carbon isotopic records is steeper than our marine record, most likely related to the upward mixing of subsurface waters with a relatively heavier carbon isotopic signature and advection processes inherent to the strong seasonality of the CCS southern boundary. These results will allow a better characterization of the relative role of the EBUS regions in the global carbon cycle.

1 Introduction

Over recent decades, the ocean has absorbed approximately 25-26% of anthropogenic CO_2 emissions from fossil fuel combustion, cement production, and land use changes, among others (Friedlingstein et al., 2025).

This uptake has slowed down the increase of atmospheric CO_2 concentrations, reducing the magnitude of the anthropogenically driven climate warming (Fung et al., 2005), and lowered the pH in surface waters with important implications for ocean acidification and marine ecosystems (Feely et al., 2004). The CO_2 exchange between the ocean and the atmosphere is driven by a combination of physical and biogeochemical processes, making an accurate sea–air CO_2 flux assessment challenging. A better understanding of these processes is necessary to improve our knowledge of the biogeochemical cycles, notably the carbon cycle, which has implications for climate change and ocean acidification (Wanninkhof et al., 2013). In this context, studies of EBUS play a key role in modulating regional air-sea CO_2 exchange. Studies have shown that these systems can act as either carbon sources or sinks, depending on the season, latitude, El Niño and La Niña events, and the arrival of marine heatwaves (Brady et al., 2019; Chikamoto and DiNezio, 2021; Feely et al., 2008; Frazão et al., 2025; Lachkar et al., 2024; Lefèvre et al., 2023; Osborne et al., 2020), making their representation in global carbon models particularly challenging.

The CO_2 released from fossil fuel combustion has a carbon isotopic composition ($\delta^{13}C$) value of -26 to -28 ‰, leading to a decline in the atmospheric $\delta^{13}C$ values from approximately -7 ‰ to -8.7 ‰ (Rubino et al., 2019). This phenomenon, known as the ^{13}C Suess effect (Keeling et al., 1979) is transferred to the ocean through air-sea exchange, and surface and subsurface water masses are the most affected by this perturbation, altering the global oceanic $\delta^{13}C$ distribution (Eide et al., 2017). Therefore, the $\delta^{13}C$ of dissolved inorganic carbon ($\delta^{13}C_{DIC}$) in surface waters is a useful tracer of oceanic uptake of anthropogenic CO_2 (hereafter referred to as C_{ant} uptake) (Sarmiento and Gruber, 2002), and has been previously used to evaluate the uptake and distribution of anthropogenic CO_2 in EBUS (Aguilera et al., 2020; Racapé et al., 2013).

In the surface ocean, biological processes preferentially take up the lighter isotope (^{12}C), shifting its $\delta^{13}C_{DIC}$ towards relatively heavier values, and thermodynamic processes tend to make the $\delta^{13}C_{DIC}$ values in cold waters moderately heavier than those in warm waters via air-sea exchange (Gruber et al., 1999). On the other hand, the uptake of atmospheric carbon by the surface ocean is progressively shifting its $\delta^{13}C_{DIC}$ towards lighter values. Gruber et al. (1999) reported a 15-year-long decrease in $\delta^{13}C$ of -0.25 ‰ per year at the time series station near Bermuda. Depth-integrated analysis from the Atlantic, Indian, and Pacific oceans also shows a decrease in the surface ocean $\delta^{13}C_{DIC}$ for the past few decades (Quay et al., 2003; Quay et al., 2007; Quay et al., 2017).

A high absolute variability in the $\delta^{13}C_{DIC}$ has been observed in the Pacific Ocean basin, linked to the spatiotemporal heterogeneity in CO_2 concentrations, phytoplankton growth rates, and biological production, all influenced by ocean mixing processes (Tagliabue and Bopp, 2008).

Studies in EBUS—such as the California, Humboldt, and Benguela Currents—have shown that $\delta^{13}C_{DIC}$ exhibits marked seasonal and regional variability. During active upwelling periods (spring–summer), the upward transport of CO_2-rich subsurface waters leads to enhanced primary productivity and remineralization, resulting in lower surface $\delta^{13}C_{DIC}$ values. Conversely, during periods of weaker upwelling, biological fixation of carbon tends to dominate, resulting in relatively higher $\delta^{13}C_{DIC}$ signatures (DeVries, 2014; Ge et al., 2022; Olsen et al., 2020). For instance, in the Humboldt Current System, intensified upwelling events have been associated with lower Sea Surface Temperature (SST) and repeated episodes of $\delta^{13}C_{DIC}$ depletion, consistent with increased contributions of remineralized carbon and reduced biological uptake during these events (Ge et al., 2022).

However, these studies are based on relatively short-term observations that began after significant fossil fuel–derived carbon had already entered the system, complicating efforts to assess the timing and magnitude of oceanic uptake. To better understand the ocean's response to increasing fossil fuel emissions since the late 19th century, it is necessary to rely on paleoceanographic proxies, as instrumental records are too recent to capture long-term trends (Berger et al., 1982). Planktic foraminifera incorporate DIC from seawater into their calcite shells in near equilibrium with the ambient $\delta^{13}C_{DIC}$ of their preferred surface ocean habitats, typically within the upper tens of meters of the water column. This process leaves a stable isotopic signature in their shells that is preserved in sediments and widely used to reconstruct past ocean circulation, carbon reservoir exchange, surface productivity, and nutrient dynamics (Broecker and Peng, 1987; Fairbanks and Wiebe, 1980; Gruber et al., 1999).

The different preferred depth habitats of planktic foraminifera have allowed for the reconstruction of the vertical water column stratification of the ocean by using geochemical proxies for temperature ($\delta^{18}O$, Mg/Ca) and for carbon proxies ($\delta^{13}C$) between near-surface and deeper-dwelling species (Berger, 1971; Emiliani, 1954; Fairbanks and Wiebe, 1980; Ravelo and Fairbanks, 1992; Sautter and Thunell, 1991; Wefer and Berger, 1991). In addition, the organic carbon $\delta^{13}C_{OC}$ also serves as a valuable proxy, as it reflects the photosynthetic conditions under which carbon was fixed, offering insights into past surface CO_2 air-sea exchange processes (Tagliabue and Bopp, 2008; Verwega et al., 2021).

The isotopic composition of the organic carbon preserved, mostly derived from phytoplankton, is linked to their physiological function (Young et al., 2013) through the fractionation of preferentially lighter ^{12}C due

to the kinetics of enzymatic processes. $\delta^{13}C_{DIC}$ and $\delta^{13}C_{OC}$ provide complementary information on carbon cycle processes and ocean-atmosphere interactions across multiple timescales. This study uses the ratio of stable isotopes for two phases of carbon, calcite in two species of planktic foraminifera living at different depths, and organic carbon preserved in marine laminated sediments from San Lazaro Basin (SLB), off Baja California, to evaluate the carbon balance between the atmosphere and surface waters in the southern domain of the CCS since the preindustrial era.

2 Materials and methods

2.1 Site description

SLB, sometimes referred to as the Soledad Basin (Soutar and Isaacs, 1974; Van Geen et al., 1995) is located off the western edge of the continental shelf off the Baja California Peninsula (25°10' N, 112°45' W) (Fig. 1). SLB is situated below the dynamic boundary between the cooler and slightly fresher CCS waters advected from the north and the relatively warmer and saltier tropical and subtropical waters from the south (Abella-Gutiérrez and Herguera, 2016). The warmer and saltier tropical and subtropical waters are associated with the poleward advection of the California surface Countercurrent close to the coast (also known as Davidson Current), whereas the subsurface nutrient- and carbon-enriched, oxygen-depleted waters originate in the equatorial region and are transported by the California Undercurrent (CUC) (Hickey, 1979).

The CCS shows a strong seasonality, characterized by an intensification of the equatorward alongshore winds during spring to early summer that intensifies the advection of the northern cooler and fresher waters of the CC and the upwelling of nutrient and carbon-enriched waters from the subsurface that fuels biological productivity (Lynn and Simpson, 1987; Sverdrup and Allen, 1939) and carbon export (Abella-Gutiérrez et al., 2020; Abella-Gutiérrez and Herguera, 2016). From late summer to early winter, the relaxation of the winds retreats the CC, which allows the invasion of warm stratified Tropical and Subtropical waters in the region, which reduces the biological productivity and carbon export (Durazo, 2015).

This seasonality is enhanced or weakened at different timescales, from interannual to multidecadal, as happens during La Niña-like conditions that extend the spring upwelling and El Niño-like conditions that enhance stratification throughout the year (Abella-Gutiérrez et al., 2020; Durazo, 2015; O'Mara et al., 2019).

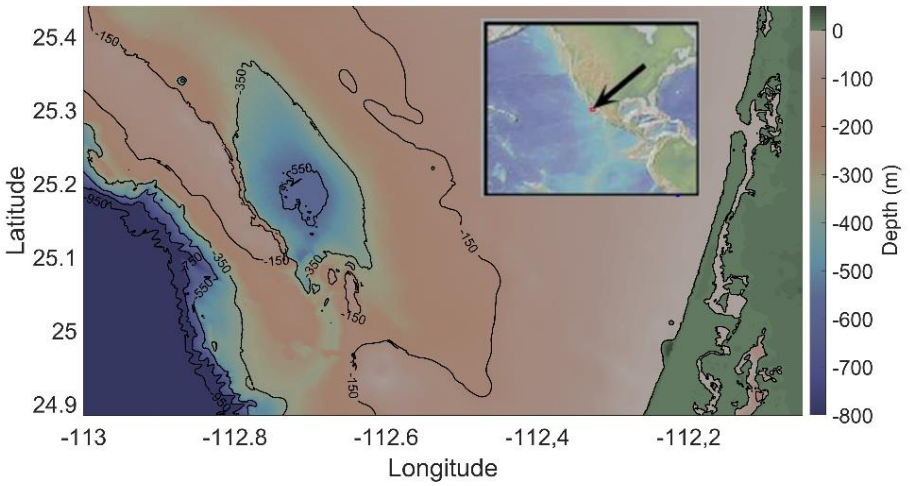


Figure 1. Localization of SLB, Baja California Sur, Mexico. The image was generated from GeoMapApp using the Global Multi-Resolution Topography (Ryan, et al., 2009) with modifications.

SLB has a maximum depth of ~540 m and is enclosed along its western margin by an uplifted branch of the Tosco-Abreojos fault system, forming a topographic barrier with depths of around 100 m that is interrupted in the southern part by a narrow sill at 350 m depth. The reduced ventilation over the sill, the oxygen-depleted waters of the CUC entering the basin through these depths, and the high productivity help to maintain the suboxic conditions on the seafloor that prevent bioturbation and enhance the preservation of the laminated sediments accumulating on its bottom (Juillet-Leclerc and Schrader, 1987; Phleger and Soutar, 1973; Thunell, 1998; Van Geen et al., 1995).

2.2 Sample collection

Two box cores (SALA11-E19MC-1 and BAP96-6C) were collected (Table 1) from the deepest part of the basin, with a Soutar-type box core that recovered a well-preserved sediment-water interface. We made further use of the top section of the Kasten core (PCM00-78K), which was previously employed in earlier studies, to describe the CCS, SST, and paleoproductivity variability (Abella-Gutiérrez et al., 2020; Abella-Gutiérrez and Herguera, 2016; O'Mara et al., 2019) to extend the record back to the preindustrial era.

After recovery, the cores were refrigerated until sampling in the lab, where they were cut into 2 cm slabs along the depth axis. Several slabs were archived and X-radiographed, and the rest were continuously sampled perpendicular to the depth axis at 2-3 mm resolution, roughly translating into 1–4 year time slices.

Two species of planktic foraminifera preserved in the sediments were selected for analysis: *Neogloboquadrina dutertrei* and *Globigerinoides ruber*. Whereas *N. dutertrei* is a non-spinose species mostly found within the upper seasonal thermocline, usually closely associated with the depth of the chlorophyll maximum in the CC (Field, 2004; Sautter and Thunell, 1991; Spindler et al., 1984), *G. ruber* is a spinose species known to host symbionts under relatively high-light conditions and to occupy a near-surface niche in the water column, where it is consistently found (Gastrich and Bartha, 1988).

Table 1. Localization and year of the collected cores in SLB

Core	Latitude	Longitude	Depth	Year	Type
SALA11-E19MC-1	25.1961 N	112.7986 W	-540 m	2011	Soutar box core
PCM00-78K	25.1883 N	112.6783 W	-540 m	2000	Kasten
BAP96-6C	25.2163 N	112.7333 W	-528 m	1996	Soutar box core

2.3 Stable isotopic determinations on carbonates and organic carbon

To determine the $\delta^{13}C_{calc}$, we used selected planktic foraminifera from cores SALA11-E19MC-1 and BAP96-6C. Freeze-dried samples were disaggregated in a solution of sodium hexametaphosphate. The sediment was washed through a 64 µm sieve mesh and then transferred and treated with a 3 % hydrogen peroxide (H_2O_2) in an ultrasonic bath for 3 minutes to help disaggregate the sediment samples to pick planktic foraminifera.

Once dried, we handpicked specimens of planktic foraminifera *N. dutertrei* and *G. ruber* from the 250-350 µm fraction; the number of specimens per species is approximately 14 shells needed to weigh a minimum total of 140 µg of carbonate per sample. These were placed in Exetainer tubes and dried at 110 °C for 24 h. Once at room temperature, the air was evacuated with ultra-pure helium (99.99 %).

After closing the Exetainer, we injected ~0.05 ml of 99 % orthophosphoric acid to dissolve the foraminifera tests, and the resulting carbon dioxide was carried with He to a gas chromatograph (GasBench II®) coupled to a DeltaPlus Advantage® mass. Each run of 45 samples was accompanied by two international reference standards, NBS19 and LSVEC, and laboratory internal references. The average precision from certified values during the runs was ±0.06 ‰ for $\delta^{13}C$ for both standards and four internal laboratory standards. Results are reported as δ values with reference to the international standard VPDB.

$$\delta^{13}C(‰) = \left(\frac{R_{sample}}{R_{standard}} - 1\right) \times 1000 \quad (1)$$

Where R is the $^{13}C/^{12}C$ ratio, and the "standard" refers to PDB belemnite.

To determine the $\delta^{13}C_{Corg}$ in the sediment samples, we analyzed 330 samples from the three cores described above. Samples were freeze-dried, and the carbonate component was dissolved with dilute hydrochloric acid (HCl). We added deionized water and centrifuged the samples to discard the supernatant, after which these were dried and encapsulated to determine their $\delta^{13}C_{Corg}$ composition.

Samples were loaded in a carousel and combusted in an oxygen atmosphere in a COSTECH elemental analyzer coupled to a Thermo DeltaV Advantage IR mass spectrometer in the *Laboratorio de Isótopos Estables* (LIE) at CICESE. Each run of 30 samples was accompanied by international reference standards USGS 40 (L-glutamic acid) and Sucrose ANU, and internal laboratory references, with average precision from certified values of ±0.06 ‰ for both standards, as well as six internal laboratory standards, reported as δ values with reference to the international standard VPDB.

$$\delta^{13}C_{Corg}(‰, VPDB) = \left(\frac{R_{sample}}{R_{standard}} - 1\right) \times 1000 \quad (2)$$

Where R is the $^{13}C/^{12}C$ ratio, and the "standard" refers to VPDB belemnite.

2.4 Age model

The absolute chronostratigraphy of core BAP96-6C was based on downcore measurements of excess ^{210}Pb (Supplementary Figure 1), from which a sedimentation rate of roughly 2.5 mm yr^{-1} was estimated (Esparza-Alvarez et al., 2007). An age of AD 1995 was assigned to the top of the core, while the bottom of the core was estimated to date to the beginning of the twentieth century. This chronological framework is consistent with the first detection of ^{137}Cs, which marks the late 1950s datum in the core. Similar sedimentation rates have been reported for another box core from the same basin (PCM00-78C), described in Abella-Gutiérrez et al. (2020).

A multicore chronostratigraphic framework for the SLB was developed by Abella-Gutiérrez et al. (2020) using X-ray lamination patterns. This framework includes several sediment cores from the basin, including the box core BAP96-6C and the Kasten core PCM00-78K. In that study, the age model was constrained using ^{210}Pb and ^{137}Cs measurements in box cores together with radiocarbon measurements from Kasten cores (Abella-Gutiérrez et al., 2020). The results of this work showed that changes in sediment density reflect productivity cycles with lower (higher) carbonate (C_{org}) content (Abella-Gutiérrez et al., 2020). These relationships allow carbonate minima (and C_{org} maxima) to be used as stratigraphic markers across cores from the basin.

To integrate the new cores SALA11-E19MC-1 into the published BAP96-6C – PCM00-78K composite, we first applied the basin-wide sedimentation rate of ~2.5 mm yr^{-1} to account for the 15-year difference between the collection of BAP96-6C (1996) and the SALA11-E19MC-1 cores (2011). This age difference corresponds to an expected stratigraphic depth offset of approximately 37.5 mm between BAP96-6C and SALA11-E19MC-1. Following this initial adjustment, the alignment was refined by correlating carbonate minima between the cores (Supplementary Figure 2).

As an independent verification of the stratigraphic alignment, we also compared variations in the Planktic foraminifera / (Planktic + Benthic foraminifera) ratio between the cores (Supplementary Figure 3). The consistency of these patterns across the correlation intervals supports the robustness of the stratigraphic correlation and suggests that any residual age uncertainty is unlikely to affect the interpretation of our results, specifically on the decadal timescales which are relevant for this paper.

2.5 Data analysis

To characterize the $\delta^{13}C$ variability in the upper water column, we analyzed $\delta^{13}C$ of *N. dutertrei* ($\delta^{13}C_{Nd}$) and *G. ruber* ($\delta^{13}C_{Gr}$), preserved in cores SALA11-E19MC-1 and BAP96-6C. The combined use of modern CO_2 observations and $\delta^{13}C$ records from species occupying different depth habitats allows for a complementary approach to assess past and present carbon cycling, providing insights into vertical variability in carbon uptake and redistribution.

Temporal trends in atmospheric and marine $\delta^{13}C$ records were evaluated using ordinary least squares regression. Differences among records were assessed using analysis of covariance (ANCOVA), with time, group, and their interaction included as explanatory variables. When significant effects were detected, pairwise comparisons were performed using Tukey-adjusted post hoc tests. To ensure comparability among datasets, regression analyses and statistical comparisons were performed using the overlapping period shared by the atmospheric and marine records. Because the atmospheric instrumental record is available from around 1980 onward, whereas the sedimentary records extend back to 1850, slope estimates, R^2 values, and statistical tests were calculated using the common interval among all records. To address different temporal scales of variability, three time windows were considered. The complete records (1850–2011) were used to characterize the long-term evolution of marine $\delta^{13}C$, whereas statistical comparisons among atmospheric and marine records were restricted to the common interval (1980–2011). Comparisons between reconstructed $\delta^{13}C_{DIC}$ and foraminiferal $\delta^{13}C$ records focused on the period after 1950, when all marine records began to show a sustained decline in $\delta^{13}C$ associated with the ^{13}C Suess effect.

We applied complementary approaches to evaluate changes in $\delta^{13}C$ in the surface ocean. First, the mean $\delta^{13}C_{Corg}$ value for the 1850–1950 interval (approximately −21‰) was used as a pre-industrial baseline to calculate anomalies in the organic carbon record. To evaluate the relationship between sedimentary organic carbon and upper-ocean dissolved inorganic carbon, $\delta^{13}C_{DIC}$ was estimated as $\delta^{13}C_{Corg}$ + 22.6‰. This isotopic offset was derived from the mean pre-industrial $\delta^{13}C_{Corg}$ value and a representative surface-water $\delta^{13}C_{DIC}$ value (+1.5 to +2.0‰) reported by Gruber et al. (1999). In addition, $\delta^{13}C_{calc}$ measured in planktic foraminifera (*G. ruber and N. dutertrei*), which approximates $\delta^{13}C_{DIC}$ at their respective calcification depths under near-equilibrium conditions, was used as an independent proxy to evaluate the consistency between inorganic and organic carbon reservoirs in recording the ^{13}C Suess effect.

3 Results

Long-term ocean-atmosphere carbon exchange

The reconstructed isotopic compositions of organic carbon from cores PCM00-78K, SALA11-E19MC-1, and BAP96-6C show minor oscillations around mean values of -21 ‰ between 1850 and 1950 and a marked trend toward more negative values as we approach the present period (Figure 2). Similarly, $\delta^{13}C_{Nd}$ and $\delta^{13}C_{Gr}$ time series exhibit a similar change towards lighter values around the 1950s.

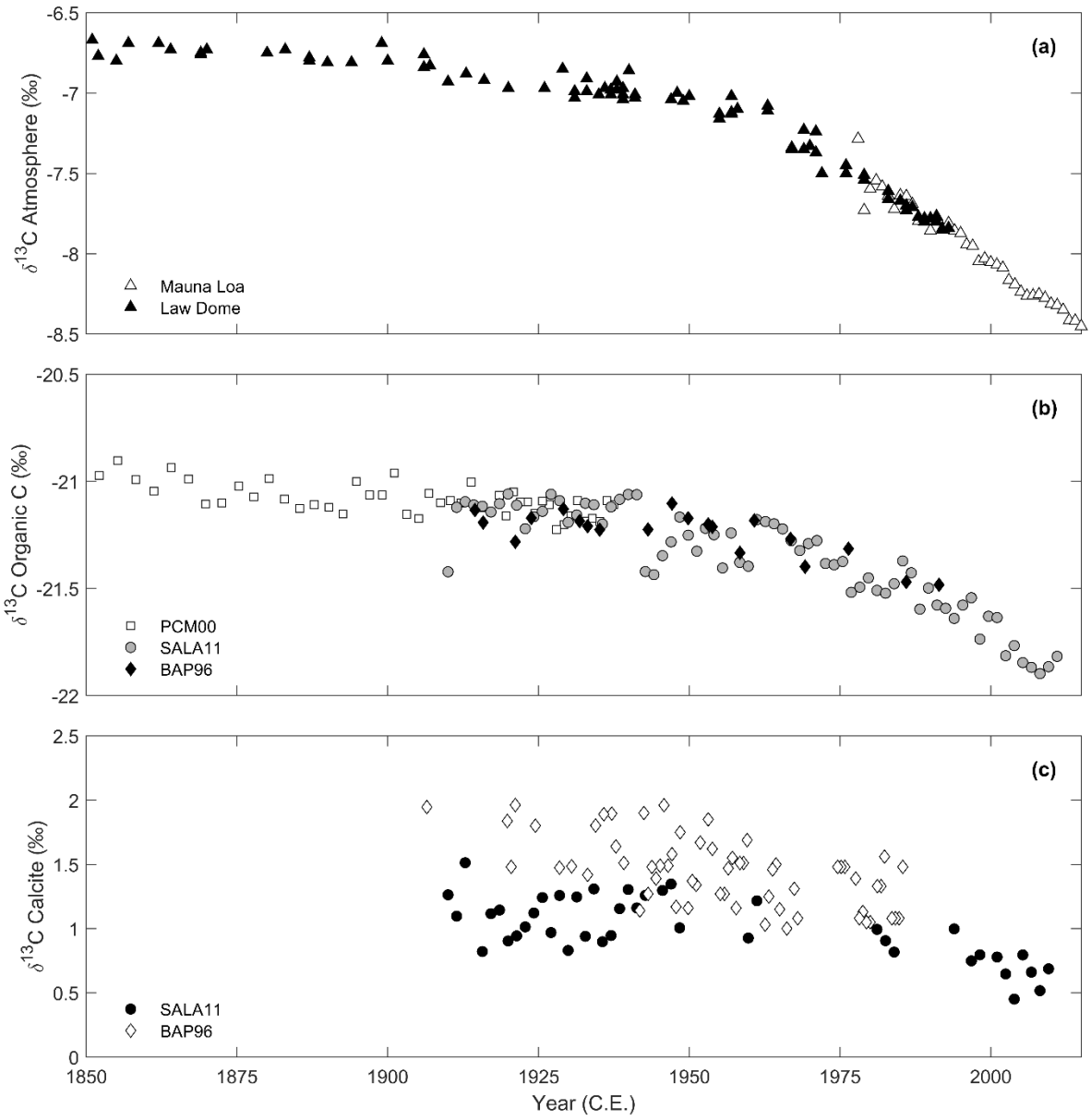


Figure 2. Time series of carbon isotopic composition from atmospheric and marine reservoirs. (a) Atmospheric $\delta^{13}C$ (‰) values derived from the Law Dome ice-core record (Rubino et al., 2019) and instrumental measurements from Mauna Loa (Keeling et al., 2005); Scripps CO_2 Program database). (b) $\delta^{13}C$ (‰) of sedimentary organic carbon from cores PCM00-78K, SALA11-E19MC-1, and BAP96-6C. (c) $\delta^{13}C$ (‰) of planktic foraminiferal calcite from *N. dutertrei* (SALA11-E19MC-1) and *G. ruber* (BAP96-6C) obtained from sediment cores.

Linear regressions show a consistent decline in $\delta^{13}C$ across all records (Figure 3). Estimated slopes indicate that the atmospheric record exhibits a significantly steeper decline (-0.261 ± 0.011 ‰ decade^{-1}; 95 % CI: -0.282 to -0.239) compared to both calcite (-0.120 ± 0.020 ‰ decade^{-1}; 95% CI: -0.160 to -0.081) and organic carbon (-0.154 ± 0.016 ‰ decade^{-1}; 95 % CI: -0.186 to -0.122). The interaction between time and

group was statistically significant ($F = 27.675$, $p = 2.02 \times 10^{-9}$), indicating that temporal trends differ among the atmospheric and marine records. The atmospheric trend differs significantly from both calcite ($p < 0.0001$) and organic carbon ($p < 0.0001$), whereas no significant difference was observed between the two marine proxies ($p = 0.3895$).

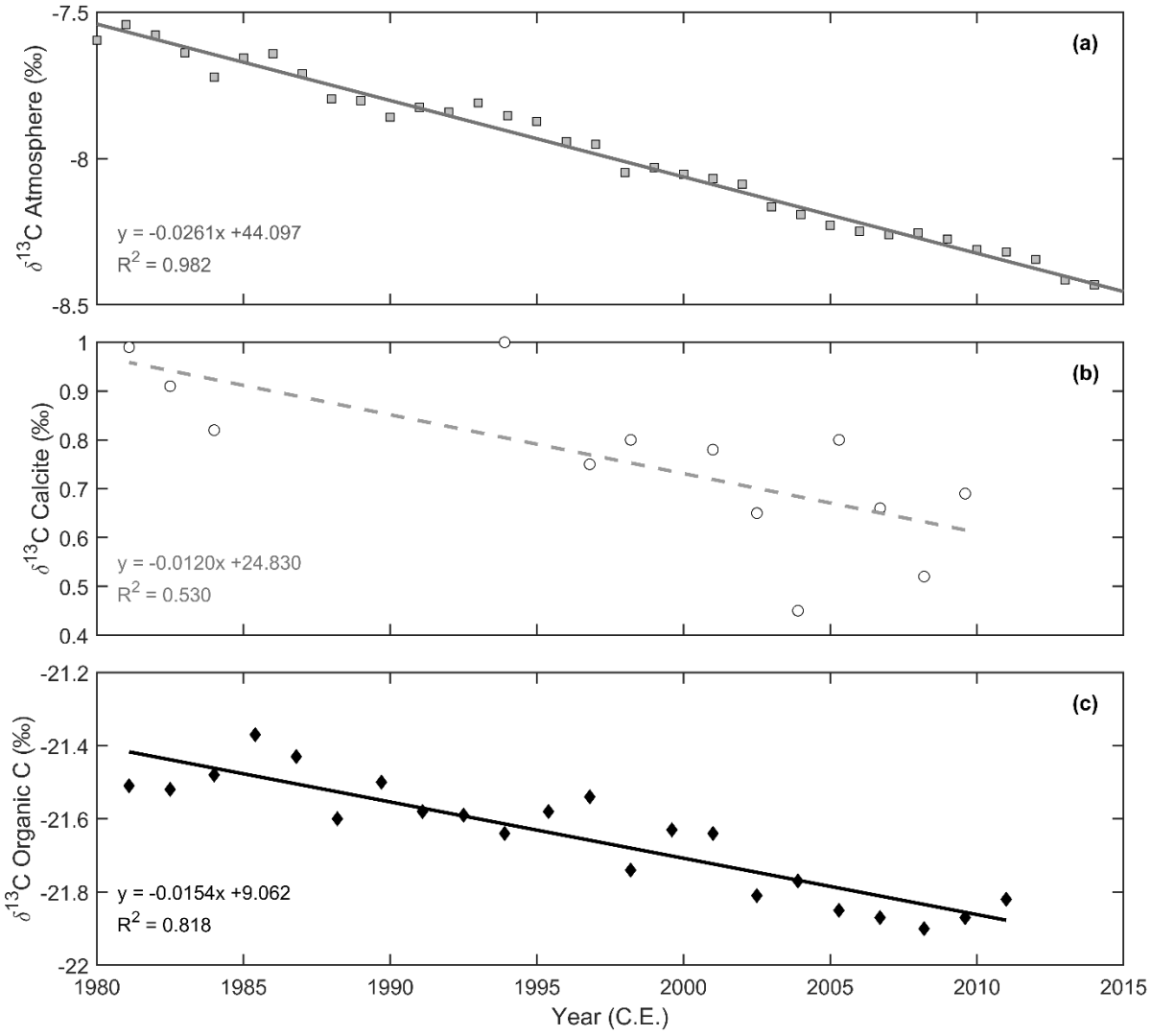


Figure 3. Linear regressions of $\delta^{13}C$ (‰) records over the common interval used for trend comparison. (a) Atmospheric $\delta^{13}C$ (‰) derived from instrumental observations. (b) $\delta^{13}C$ of planktic foraminiferal calcite from *N. dutertrei*. (c) $\delta^{13}C$ (‰) of sedimentary organic carbon. Regression equations and corresponding R^2 values are shown in each panel.

Reconstructed $\delta^{13}C_{DIC}$ values consistently fall between the $\delta^{13}C$ values recorded by *G. ruber* and *N. dutertrei* and exhibit a long-term decrease toward the present, similar to that observed in both foraminiferal

242 records (Figure 4). The close correspondence among these records suggests that the long-term trend
243 observed in $\delta^{13}C_{Corg}$ captures variability in upper-ocean $\delta^{13}C_{DIC}$.

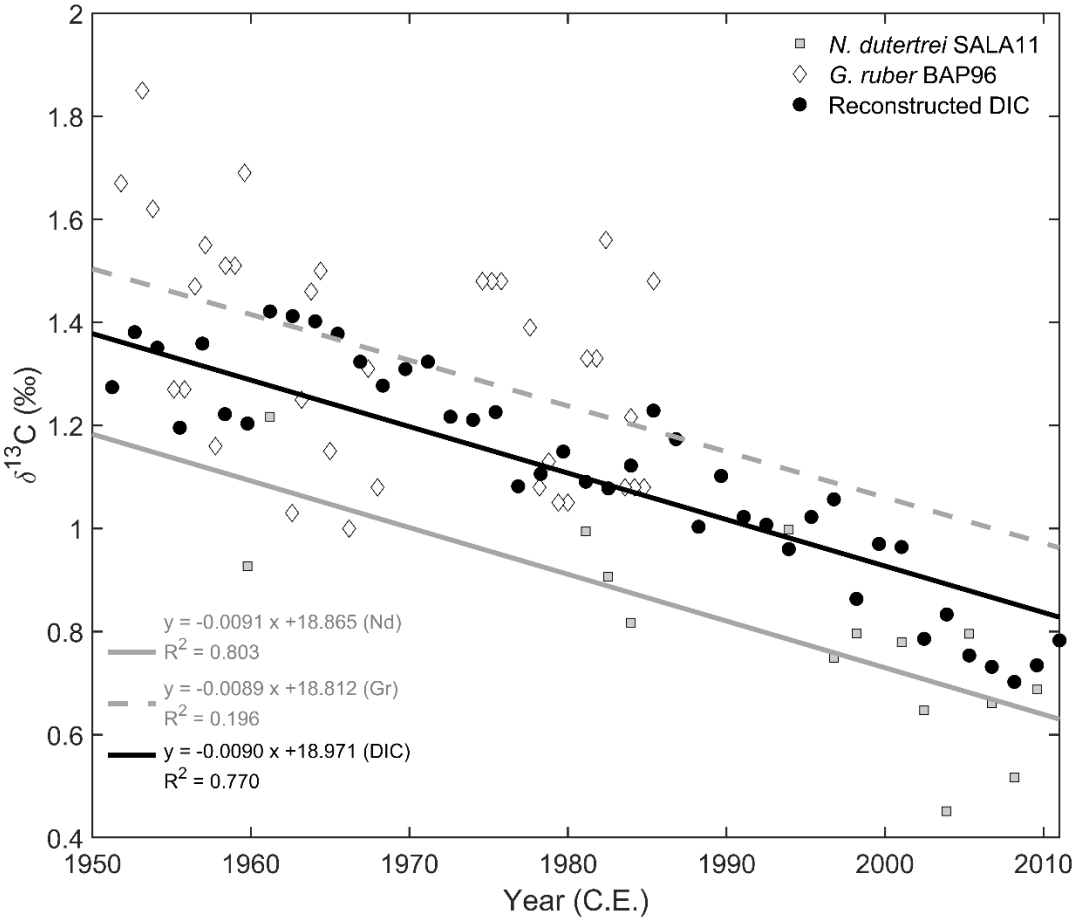


Figure 4. Time series and trends of the carbon isotopic composition of *G. ruber* (‰) (open diamonds) and *N. dutertrei* (‰) (black circles), as well as the DIC (‰) (grey squares), are derived from organic carbon in the sediments.

244 **4 Discussions**

245 The reconstructed $\delta^{13}C$ of both organic carbon and calcite follows similar decreasing trends to the observed
246 (Keeling et al., 2005) and reconstructed (Rubino et al., 2019) values of the atmosphere (Figure 2), associated
247 with the ^{13}C Suess effect, driven by the combustion of fossil fuels (Keeling et al., 1979, 2005; Tans, 2022).
248 However, the shallower slope found in our proxies ($\delta^{13}C_{Corg}$ and $\delta^{13}C_{Nd}$) suggests other processes are
249 involved, most likely related to the seasonal source and sink roles of EBUS regions on the carbon cycle.

250 In addition to the long-term decline, our records indicate a marked shift in $\delta^{13}C$ trends beginning in the
251 mid-twentieth century, particularly around the 1950s, coinciding with the accelerated rise in atmospheric

CO_2 documented in the Law Dome ice-core record. This timing is consistent with the well-documented post-World War II increase in fossil-fuel emissions and suggests that the onset of a stronger anthropogenic carbon signal is recorded in both the organic and carbonate phases. A similar transition is less clearly expressed in planktic foraminiferal $\delta^{13}C$ records from the CCS (Osborne et al., 2020), despite independent evidence for declining carbonate ion concentrations beginning in the late 1940s and 1950s. This discrepancy has been attributed to carbonate chemistry effects that may bias foraminiferal $\delta^{13}C$ toward heavier values under undersaturated conditions (Spero et al., 1997), potentially masking part of the atmospheric signal. However, recent paleoceanographic evidence suggests that the carbonate ion effect observed in laboratory experiments may not be preserved in planktic foraminiferal $\delta^{13}C$ records (Köhler and Mulitza, 2024). In contrast, the presence of a comparable mid-century shift in our organic carbon $\delta^{13}C$ record, which is not affected by carbonate-related fractionation during calcification, supports the interpretation that this feature reflects a surface-ocean response to the increasing atmospheric CO_2 burden rather than an artifact of foraminiferal calcification processes. The emergence of this signal in both proxies suggests that the propagation of the ^{13}C Suess effect into surface waters was already detectable in the CCS by the mid-twentieth century, although subsequently modulated by regional oceanographic processes.

This regional modulation is particularly important in EBUS. Influenced by seasonal upwelling, our study area represents a complex setting for interpreting $\delta^{13}C$ variability. Upwelling introduces relatively heavier $\delta^{13}C$ DIC-rich waters to the surface ocean, potentially buffering the lighter isotopic composition of atmospheric CO_2 ($\delta^{13}C_{atm}$) of the ^{13}C Suess effect (Quay et al., 2017; Tagliabue and Bopp, 2008). In these regions, $\delta^{13}C$ values in surface waters are controlled on the one hand by air–sea CO_2 exchange and by respiration processes of organic matter and the DIC content of upwelled waters. As observed in our proxy records, this mixture of sources most likely leads to $\delta^{13}C$ signals that diverge from atmospheric trends, particularly in eastern boundary current systems like the California Current.

An additional source of uncertainty in the interpretation of planktic foraminiferal $\delta^{13}C$ records is the potential variability in calcification depth through time. In particular, *N. dutertrei* commonly inhabits waters near the chlorophyll maximum and may shift its preferred habitat in response to changes in upwelling intensity, thermocline depth, and upper-ocean stratification. Such vertical habitat migration could influence the recorded $\delta^{13}C$ signal independently of atmospheric forcing by exposing the species to different portions of the water-column $\delta^{13}C$ gradient. However, although interannual and decadal fluctuations in habitat depth are expected in the California Current System, both *N. dutertrei* and *G. ruber* exhibit comparable long-term trends toward lighter $\delta^{13}C$ values. This suggests that potential changes in calcification depth are unlikely to

be the primary driver of the observed secular decline and instead represent a secondary source of variability superimposed on the long-term isotopic signal.

Consistent with this interpretation, the trends observed in our study fall within the range previously reported for regions influenced by the oceanic expression of the ^{13}C Suess effect. The $\delta^{13}C_{calc}$ values of planktic foraminifera calcite show a slope of -0.12‰ per decade since 1980, while the $\delta^{13}C_{Corg}$ shows a slope of -0.15‰ per decade. These values lie at the low range of variability previously reported of -0.20±0.06 decade^{-1} for the North Pacific, which is already lower than the 0.27‰ decade^{-1} observed for the atmospheric CO_2 (Quay et al., 2017). According to Gruber et al. (1999) the highest ^{13}C Suess effect, -0.25 ‰ decade^{-1}, is found in the subtropical gyres such as Bermuda and Hawaii, whereas the lowest, -0.15 ‰ decade^{-1}, is found in the equatorial Pacific upwelling region. Our study region shows a decreasing decadal trend similar to the equatorial region, characteristic of its strong upwelling. Although temperature-dependent fractionation and total CO_2 fluxes are relevant, most observed trends towards lighter values in the surface ocean $\delta^{13}C_{DIC}$ can be attributed to the input of $\delta^{13}C_{atm}$. Therefore, understanding the spatial distribution of the ^{13}C Suess effect requires considering ocean mixing and circulation patterns (Tagliabue and Bopp, 2008).

Surface ocean $\delta^{13}C$ is mainly controlled by the input of atmospheric CO_2, either through air–sea exchange or lateral advection of anthropogenic CO_2, the export of organic matter, respiration processes in the surface layer, the lateral advection of DIC, and mixing from subsurface waters. This intrusion of isotopically light atmospheric CO_2 into the ocean tends to erase natural $\delta^{13}C$ gradients (Eide et al., 2017), and consequently the variability of the $\delta^{13}C_{DIC}$ downstream of upwelling zones introduced by primary productivity, upwelling of older water, and $\delta^{13}C_{atm}$ (Tagliabue and Bopp, 2008). Consistent with this interpretation, Eide et al. (2017) showed that the magnitude of the oceanic ^{13}C Suess effect is reduced in regions characterized by strong vertical mixing and upwelling, where the continuous supply of aged, carbon-rich subsurface waters attenuates the atmospheric isotopic signal. Our results coincide with this pattern, as both $\delta^{13}C_{Calc}$ and $\delta^{13}C_{Corg}$ show attenuated decreasing trends relative to atmospheric CO_2, supporting the interpretation that regional upwelling dynamics and ocean circulation modulate the propagation of the anthropogenic $\delta^{13}C$ signal to the ocean surface.

The atmospheric record exhibits a decline of −0.261‰ decade^{-1}, whereas the marine records show declines ranging from −0.120 to −0.154‰ decade^{-1}, indicating an attenuation of approximately 0.11–0.14‰ decade^{-1} relative to the atmospheric signal. However, a quantitative partitioning among subsurface mixing, air–sea exchange, and biological processes is not possible with the available proxy records. In EBUS, these mechanisms are tightly coupled and collectively influence surface-water DIC and $\delta^{13}C$. Recent observations

from the California Current System (Frazão et al., 2025) demonstrate that changes in upwelling intensity and water-mass composition can alter air–sea CO_2 exchange and surface carbon inventories, highlighting the difficulty of attributing the observed $\delta^{13}C$ attenuation to any single process. Therefore, the observed attenuation provides an estimate of the total oceanic modulation of the atmospheric signal, while the reduced slopes recorded in our proxies likely reflect the integrated response of the upper-ocean carbon cycle to multiple interacting physical and biogeochemical processes.

Against this background of interacting controls, biological fractionation may also contribute to the observed differences between atmospheric and marine $\delta^{13}C$ trends. SST have been shown to be related to a suite of environmental variables in our study region, such as upper ocean mixing, nutrients, and primary productivity (Abella-Gutiérrez and Herguera, 2016; Durazo, 2015). It also has a well-known relationship with CO_2 concentrations in the water column (Weiss, 1974) and with the fractionation of carbon isotopes between the DIC in the water column and phytoplankton biomass. This fractionation, known as the biological fractionation factor (Freeman and Hayes, 1992), has been reported to change by phytoplankton in the surface ocean in a well-resolved time series study of phytoplankton $\delta^{13}C$ in the subtropical Atlantic, showing how the isotopic composition of the POC trended towards lighter values than the atmospheric CO_2 trend (Young et al., 2013). They hypothesized that the anthropogenic CO_2 emissions and the consequent increase in the availability of inorganic carbon in the water column are changing the fractionation toward lighter values (Young et al., 2013). However, they cannot rule out the importance of other factors such as carbon fixation, CO_2-specific uptake, and HCO_3^- use (Young et al., 2013).

Young et al., (2013) state that this biological fractionation is controlled by intracellular Rayleigh fractionation and that the sensitivity of this fractionation could decrease with increasing CO_2 concentrations, which explains the differences in the fractionation trends between the subtropics and the tropics. There is clear evidence of higher CO_2 uptake in the CCS (Frazão et al., 2025; Wolfe et al., 2023), and that these eastern boundary current waters already have relatively high DIC values brought by enriched subsurface carbon, nutrient, and CO_2 old waters, which may push biological fractionation to the minimum values observed for the tropics of 0.01‰ $year^{-1}$ (Young et al., 2013). Although long-term DIC and alkalinity records are not available for SLB, a simple sensitivity estimate can be made using the fractionation changes proposed by Young et al., (2013). Applying an additional isotopic fractionation of approximately 0.10‰ $decade^{-1}$ to the atmospheric $\delta^{13}C_{CO2}$ trend would result in an expected decline of about -0.36‰ $decade^{-1}$ (-0.26‰ $decade^{-1}$ from the atmosphere plus -0.10‰ $decade^{-1}$ from enhanced biological fractionation). This predicted trend is substantially steeper than the declines observed in either $\delta^{13}C_{Corg}$ or $\delta^{13}C_{calc}$. Therefore, changes in biological fractionation alone cannot explain the isotopic trends observed in our records,

indicating that multiple processes influence the propagation of the atmospheric $\delta^{13}C$ signal into the surface ocean.

Our results show this mixture of influences, as our proxies are partially tracking the atmospheric signal. Tracking the propagation of the ^{13}C Suess effect across Earth system components offers insights into the magnitude of anthropogenic CO_2 sinks (Eide et al., 2017). Gruber et al., (1999) estimated that the global oceanic ^{13}C Suess effect closely matches the atmospheric trend. In contrast, Tagliabue and Bopp (2008) reported $\delta^{13}C_{DIC}$ decline rates of −0.07‰ per decade between 1860 and 2000, increasing to −0.18‰ per decade between 1970 and 2000. Published estimates for 1970–1990 show ocean $\delta^{13}C_{DIC}$ changes of −0.15 to −0.171‰ per decade, representing roughly 65% of the $\delta^{13}C_{atm}$ decrease (Quay et al., 2003; Sonnerup et al., 1999).

Although atmospheric inputs primarily drive the propagation of the ^{13}C Suess effect into the surface ocean, its oceanic expression is modulated by regional circulation, upwelling dynamics, and biological productivity. For instance, the upwelling of older, relatively heavier $\delta^{13}C$ deep waters, as observed in our study area, can offset the surface signal. If fossil-fuel-driven atmospheric changes were the only process involved, $\delta^{13}C_{Corg}$ and $\delta^{13}C_{Nd}$ would closely follow atmospheric trends. Upwelling delivers remineralized DIC with a heavier $\delta^{13}C$ than the atmosphere, and the magnitude of this effect depends on the age and origin of the water mass. This dual effect may partially buffer the surface ^{13}C Suess signal in regions such as the California Current (Quay et al., 2017; Tagliabue and Bopp, 2008). The mismatch in slope between atmospheric and marine $\delta^{13}C$ records reflects the role of other oceanic processes, such as lateral and subsurface mixing with the upper ocean mixed layer, as well as the integration of multiple carbon pools, including organic matter, upper ocean DIC, and pathways driven by biological productivity in the surface waters. Our data reinforce that sedimentary $\delta^{13}C$ reflects a regional imprint of global carbon cycle perturbations, modulated by local oceanographic processes.

Similar behavior has been reported in other studies of the CCS, highlighting the complexity of interpreting $\delta^{13}C$ trends in upwelling-dominated environments. Osborne et al., (2020) reconstructed surface-ocean acidification over the last century and documented substantial declines in carbonate ion concentration and pH, yet observed relatively weak $\delta^{13}C$ trends in planktic foraminifera. The steepest decline reported in their study, recorded by *G. bulloides*, was approximately −0.07‰ decade^{-1}, lower than the trends observed here. They proposed that carbonate undersaturation may bias foraminiferal $\delta^{13}C$ toward heavier values, partially masking the atmospheric $\delta^{13}C$ signal. In our records, however, the similar mid-century transition observed

in both carbonate and organic carbon phases suggests that the long-term trend cannot be explained solely by carbonate chemistry effects (Osborne et al., 2020).

Additional insight comes from recent observations of carbon cycling in the CCS. Frazão et al., (2025) showed that nearshore waters can alternate between acting as a source and a sink of atmospheric CO_2 depending on upwelling intensity, thermocline depth, and marine heatwave occurrence. During periods of strong upwelling, old carbon-rich subsurface waters dominate surface-water DIC and pCO_2, promoting CO_2 outgassing, whereas reduced upwelling during El Niño events and marine heatwaves can temporarily reverse this balance (Frazão et al., 2025). These observations emphasize that the isotopic evolution of surface-water DIC reflects the combined effects of anthropogenic carbon uptake, air-sea exchange, biological cycling, and the recurrent introduction of subsurface waters.

A recent study has also highlighted the importance of thermodynamic buffering in amplifying the effects of remineralization on subsurface dissolved inorganic carbon inventories (Stoll et al., 2025). Such nonlinear processes further complicate the relationship between ocean acidification and carbon isotope variability and underscore the importance of water-mass history when interpreting long-term biogeochemical change. Within this framework, sedimentary $\delta^{13}C$ records may be particularly valuable as indicators of the propagation of the ^{13}C Suess effect through surface waters, even when multiple regional processes modulate the magnitude of the observed signal. Upwelling regions like the Southern California Current play a central role in shaping the marine isotopic carbon signal. The persistence of seasonal source/sink behavior in surface waters likely contributes to the lower slope observed in sediment $\delta^{13}C$ values. Although the ^{13}C Suess effect dominates the long-term trend, its regional expression depends on the balance between atmospheric CO_2 uptake and the delivery of older DIC from depth. As Le Quéré et al. (2018) emphasize regional systems with dynamic vertical and horizontal transport processes are key components of the global carbon cycle and crucial to understanding the propagation of anthropogenic CO_2 through the ocean-atmosphere system.

4 Conclusions

The $\delta^{13}C$ trends of planktic foraminifera calcite and organic carbon in our study, with slopes of −0.12‰ and −0.15‰ per decade, respectively (Figure 3), lie at the lower end of the variability reported for the North Pacific, although similar to the decadal rates reported for the equatorial Pacific, and remain consistently below the $\delta^{13}C_{atm}$ trend. These findings reflect the global imprint of the ^{13}C Suess effect and the influence of regional oceanographic processes such as mixing of subsurface waters driven by upwelling processes.

The observed differences in the $\delta^{13}C$ trends in planktic foraminifera and organic carbon with respect to the atmospheric trend suggest a combined effect of anthropogenic atmospheric CO_2 source and the upwelling of intermediate waters with relatively enriched $\delta^{13}C$ signatures compared to atmospheric values, in the California Current. These mechanisms modulate the isotopic imprint of atmospheric CO_2 on the ocean, leading to spatial heterogeneity in the marine $\delta^{13}C$ response.

Temporal patterns further confirm that the oceanic $\delta^{13}C$ response partially buffers the atmospheric trend, highlighting the role of ocean circulation and ventilation timescales. The discrepancy between sediment $\delta^{13}C$ records (Figure 3) and atmospheric ones underscores the need to consider the integration of multiple carbon pools and processes—such as biological export, remineralization, and lateral transport—when interpreting long-term isotopic trends in the ocean sediment records.

Our results emphasize the importance of the anthropogenic source of carbon in altering the oceanic carbon isotopic composition and how this trend has significantly shifted in the CCS since the 1950s, mirroring the atmospheric CO_2 trend recorded in ice core records (e.g., Law Dome, Antarctica) and continued into the instrumental record.

Author contributions

YVCP: First author, laboratory and data analysis, data curation, and conceptualization. JLAG: Data analysis and writing. GVE: Data analysis and writing. JCHG: Conceptualization, supervision, investigation, methodology, data curation, resources, project administration, funding acquisition, writing-review and editing, manuscript improvement. All authors contributed to the article and approved the submitted version.

Funding

Y.V. Contreras-Pacheco was supported by a CONAHCYT Master's and PhD fellowship.

Acknowledgments

We thank Cynthia Nava, Bertha Acosta, Axel Rosas, Aidé Egremy, Mireya Montero, Nathali Cordero, and Doreny Bobadilla for their help in the collection and the laboratory work. We also thank Gerardo Quintanilla for his feedback during the earlier stages. We thank the crew of the R/V Francisco Ulloa for their support. This study has been conducted using E.U. Copernicus Marine Service Information.

Competing interests

The contact author has declared that none of the authors have any competing interests.

References

Abella-Gutiérrez, J. and Herguera, J. C.: Sensitivity of carbon paleoproductivity in the Southern California Current System on different time scales for the last 2 ka: Carbon Paleoproductivity in the Southern CCS, Paleoceanography, 31, 953–970, https://doi.org/10.1002/2015PA002872, 2016.

Abella-Gutiérrez, J., Herguera, J. C., Mortyn, P. G., Kelly, C. S., and Martínez-Botí, M. A.: Multidecadal Climate Variability in the Southern Region of the California Current System During the Last 1,800 Years, Paleoceanogr. Paleoclimatology, 35, e2019PA003825, https://doi.org/10.1029/2019PA003825, 2020.

Aguilera, V. M., Vargas, C. A., and Dewitte, B.: Intraseasonal Hydrographic Variations and Nearshore Carbonates System Off Northern Chile During the 2015 El Niño Event, J. Geophys. Res. Biogeosciences, 125, e2020JG005704, https://doi.org/10.1029/2020JG005704, 2020.

Berger, W., Bonneau, M., and Parker, F.: Foraminifera on the deep-sea floor - lysocline and dissolution rate, Oceanol. Acta, 5, 249–258, 1982.

Berger, W. H.: Sedimentation of planktonic foraminifera, Mar. Geol., 11, 325–358, https://doi.org/10.1016/0025-3227(71)90035-1, 1971.

Brady, R. X., Lovenduski, N. S., Alexander, M. A., Jacox, M., and Gruber, N.: On the role of climate modes in modulating the air–sea CO_2 fluxes in eastern boundary upwelling systems, Biogeosciences, 16, 329–346, https://doi.org/10.5194/bg-16-329-2019, 2019.

Broecker, W. S. and Peng, T.-H.: The role of $CaCO_3$ compensation in the glacial to interglacial atmospheric CO_2 change, Glob. Biogeochem. Cycles, 1, 15–29, https://doi.org/10.1029/GB001i001p00015, 1987.

Chikamoto, M. O. and DiNezio, P.: Multi-Century Changes in the Ocean Carbon Cycle Controlled by the Tropical Oceans and the Southern Ocean, Glob. Biogeochem. Cycles, 35, e2021GB007090, https://doi.org/10.1029/2021GB007090, 2021.

DeVries, T.: The oceanic anthropogenic CO_2 sink: Storage, air-sea fluxes, and transports over the industrial era, Glob. Biogeochem. Cycles, 28, 631–647, https://doi.org/10.1002/2013GB004739, 2014.

Durazo, R.: Seasonality of the transitional region of the California Current System off Baja California, J. Geophys. Res. Oceans, 120, 1173–1196, https://doi.org/10.1002/2014JC010405, 2015.

Eide, M., Olsen, A., Ninnemann, U. S., and Eldevik, T.: A global estimate of the full oceanic ^{13}C Suess effect since the preindustrial, Glob. Biogeochem. Cycles, 31, 492–514, https://doi.org/10.1002/2016GB005472, 2017.

Emiliani, C.: Depth habitats of some species of pelagic Foraminifera as indicated by oxygen isotope ratios, Am. J. Sci., 252, 149–158, https://doi.org/10.2475/ajs.252.3.149, 1954.

Esparza-Alvarez, M. A., Herguera, J. C., and Lange, C.: Last century patterns of sea surface temperatures and diatom (>38 μm) variability in the Southern California current, Mar. Micropaleontol., 64, 18–35, https://doi.org/10.1016/j.marmicro.2007.01.001, 2007.

Fairbanks, R. G. and Wiebe, P. H.: Foraminifera and Chlorophyll Maximum: Vertical Distribution, Seasonal Succession, and Paleoceanographic Significance, Science, 209, 1524–1526, https://doi.org/10.1126/science.209.4464.1524, 1980.

Feely, R. A., Sabine, C. L., Lee, K., Berelson, W., Kleypas, J., Fabry, V. J., and Millero, F. J.: Impact of Anthropogenic CO_2 on the $CaCO_3$ System in the Oceans, Science, 305, 362–366, https://doi.org/10.1126/science.1097329, 2004.

Feely, R. A., Sabine, C. L., Hernandez-Ayon, J. M., Ianson, D., and Hales, B.: Evidence for Upwelling of Corrosive "Acidified" Water onto the Continental Shelf, Science, 320, 1490–1492, https://doi.org/10.1126/science.1155676, 2008.

Field, D. B.: Variability in vertical distributions of planktonic foraminifera in the California Current: Relationships to vertical ocean structure: Vertical Variability of Foraminifera, Paleoceanography, 19, n/a-n/a, https://doi.org/10.1029/2003PA000970, 2004.

Frazão, L., Tonelli, M., and Signori, C.: Long-term responses of microbial plankton to ocean warming reveal shifts in air–sea CO_2 exchange in the late 21st century, https://doi.org/10.21203/rs.3.rs-7284245/v1, 12 August 2025., 2025.

Freeman, K. H. and Hayes, J. M.: Fractionation of carbon isotopes by phytoplankton and estimates of ancient CO_2 levels, Glob. Biogeochem. Cycles, 6, 185–198, https://doi.org/10.1029/92GB00190, 1992.

Friedlingstein, P., O'Sullivan, M., Jones, M. W., Andrew, R. M., Hauck, J., Landschützer, P., Le Quéré, C., Li, H., Luijkx, I. T., Olsen, A., Peters, G. P., Peters, W., Pongratz, J., Schwingshackl, C., Sitch, S., Canadell, J. G., Ciais, P., Jackson, R. B., Alin, S. R., Arneth, A., Arora, V., Bates, N. R., Becker, M., Bellouin, N., Berghoff, C. F., Bittig, H. C., Bopp, L., Cadule, P., Campbell, K., Chamberlain, M. A., Chandra, N., Chevallier, F., Chini, L. P., Colligan, T., Decayeux, J., Djeutchouang, L. M., Dou, X., Duran Rojas, C., Enyo, K., Evans, W., Fay, A. R., Feely, R. A., Ford, D. J., Foster, A., Gasser, T., Gehlen, M., Gkritzalis, T., Grassi, G., Gregor, L., Gruber, N., Gürses, Ö., Harris, I., Hefner, M., Heinke, J., Hurtt, G. C., Iida, Y., Ilyina, T., Jacobson, A. R., Jain, A. K., Jarníková, T., Jersild, A., Jiang, F., Jin, Z., Kato, E., Keeling, R. F., Klein Goldewijk, K., Knauer, J., Korsbakken, J. I., Lan, X., Lauvset, S. K., Lefèvre, N., Liu, Z., Liu, J., Ma, L., Maksyutov, S., Marland, G., Mayot, N., McGuire, P. C., Metzl, N., Monacci, N. M., Morgan, E. J., Nakaoka, S.-I., Neill, C., Niwa, Y., Nützel, T., Olivier, L., Ono, T., Palmer, P. I., Pierrot, D., Qin, Z., Resplandy, L., Roobaert, A., Rosan, T. M., Rödenbeck, C., Schwinger, J., Smallman, T. L., Smith, S. M., Sospedra-Alfonso, R., Steinhoff, T., Sun, Q., Sutton, A. J., Séférian, R., Takao, S., Tatebe, H., Tian, H., Tilbrook, B., Torres, O., Tourigny, E., Tsujino, H., Tubiello, F., Van Der Werf, G., Wanninkhof, R., Wang, X., Yang, D., Yang, X., Yu, Z., Yuan, W., Yue, X., Zaehle, S., Zeng, N., and Zeng, J.: Global Carbon Budget 2024, Earth Syst. Sci. Data, 17, 965–1039, https://doi.org/10.5194/essd-17-965-2025, 2025.

Fung, I. Y., Doney, S. C., Lindsay, K., and John, J.: Evolution of carbon sinks in a changing climate, Proc. Natl. Acad. Sci., 102, 11201–11206, https://doi.org/10.1073/pnas.0504949102, 2005.

Gastrich, M. D. and Bartha, R.: Primary productivity in the planktonic foraminifer *Globigerinoides ruber* (d'Orbigny), J. Foraminifer. Res., 18, 137–142, https://doi.org/10.2113/gsjfr.18.2.137, 1988.

Ge, T., Luo, C., Ren, P., Zhang, H., Fan, D., Chen, H., Chen, Z., Zhang, J., and Wang, X.: Stable carbon isotopes of dissolved inorganic carbon in the Western North Pacific Ocean: Proxy for water mixing and dynamics, Front. Mar. Sci., 9, 998437, https://doi.org/10.3389/fmars.2022.998437, 2022.

Gruber, N., Keeling, C. D., Bacastow, R. B., Guenther, P. R., Lueker, T. J., Wahlen, M., Meijer, H. A. J., Mook, W. G., and Stocker, T. F.: Spatiotemporal patterns of carbon-13 in the global surface oceans and the oceanic suess effect, Glob. Biogeochem. Cycles, 13, 307–335, https://doi.org/10.1029/1999GB900019, 1999.

Hickey, B. M.: The California current system—hypotheses and facts, Prog. Oceanogr., 8, 191–279, https://doi.org/10.1016/0079-6611(79)90002-8, 1979.

Juillet-Leclerc, A. and Schrader, H.: Variations of upwelling intensity recorded in varved sediment from the Gulf of California during the past 3,000 years, Nature, 329, 146–149, https://doi.org/10.1038/329146a0, 1987.

Keeling, C. D., Mook, W. G., and Tans, P. P.: Recent trends in the $^{13}C/^{12}C$ ratio of atmospheric carbon dioxide, Nature, 277, 121–123, https://doi.org/10.1038/277121a0, 1979.

Keeling, C. D., Piper, S. C., Bacastow, R. B., Wahlen, M., Whorf, T. P., Heimann, M., and Meijer, H. A.: Atmospheric CO_2 and $^{13}CO_2$ exchange with the terrestrial biosphere and oceans from 1978 to 2000: observations and carbon cycle implications, in: A History of Atmospheric CO_2 and its effects on Plants, Animals, and Ecosystems, Springer Verlag, New York, 83–113, 2005.

Köhler, P. and Mulitza, S.: No detectable influence of the carbonate ion effect on changes in stable carbon isotope ratios ($\delta^{13}C$) of shallow dwelling planktic foraminifera over the past 160 kyr, Clim. Past, 20, 991–1015, https://doi.org/10.5194/cp-20-991-2024, 2024.

Lachkar, Z., Cornejo-D'Ottone, M., Singh, A., Arístegui, J., Dewitte, B., Fawcett, S., Garçon, V., Lovecchio, E., Molina, V., and Vinayachandran, P. N. M.: Biogeochemistry of greenhouse gases in coastal upwelling systems: Processes and sensitivity to global change, Elem Sci Anth, 12, 00088, https://doi.org/10.1525/elementa.2023.00088, 2024.

Le Quéré, C., Andrew, R. M., Friedlingstein, P., Sitch, S., Hauck, J., Pongratz, J., Pickers, P. A., Korsbakken, J. I., Peters, G. P., Canadell, J. G., Arneth, A., Arora, V. K., Barbero, L., Bastos, A., Bopp, L., Chevallier, F., Chini, L. P., Ciais, P., Doney, S. C., Gkritzalis, T., Goll, D. S., Harris, I., Haverd, V., Hoffman, F. M., Hoppema, M., Houghton, R. A., Hurtt, G., Ilyina, T., Jain, A. K., Johannessen, T., Jones, C. D., Kato, E., Keeling, R. F., Goldewijk, K. K., Landschützer, P., Lefèvre, N., Lienert, S., Liu, Z., Lombardozzi, D., Metzl, N., Munro, D. R., Nabel, J. E. M. S., Nakaoka, S., Neill, C., Olsen, A., Ono, T., Patra, P., Peregon, A., Peters, W., Peylin, P., Pfeil, B., Pierrot, D., Poulter, B., Rehder, G., Resplandy, L., Robertson, E., Rocher, M., Rödenbeck, C., Schuster, U., Schwinger, J., Séférian, R., Skjelvan, I., Steinhoff, T., Sutton, A., Tans, P. P., Tian, H., Tilbrook, B., Tubiello, F. N., Van Der Laan-Luijkx, I. T., Van Der Werf, G. R., Viovy, N., Walker, A. P., Wiltshire, A. J., Wright, R., Zaehle, S., and Zheng, B.: Global Carbon Budget 2018, Earth Syst. Sci. Data, 10, 2141–2194, https://doi.org/10.5194/essd-10-2141-2018, 2018.

Lefèvre, N., Veleda, D., and Hartman, S. E.: Outgassing of CO_2 dominates in the coastal upwelling off the northwest African coast, Deep Sea Res. Part Oceanogr. Res. Pap., 200, 104130, https://doi.org/10.1016/j.dsr.2023.104130, 2023.

Lynn, R. J. and Simpson, J. J.: The California Current system: The seasonal variability of its physical characteristics, J. Geophys. Res., 92, 12947, https://doi.org/10.1029/JC092iC12p12947, 1987.

Olsen, A., Lange, N., Key, R. M., Tanhua, T., Bittig, H. C., Kozyr, A., Álvarez, M., Azetsu-Scott, K., Becker, S., Brown, P. J., Carter, B. R., Cotrim Da Cunha, L., Feely, R. A., Van Heuven, S., Hoppema, M., Ishii, M., Jeansson, E., Jutterström, S., Landa, C. S., Lauvset, S. K., Michaelis, P., Murata, A., Pérez, F. F.,

Pfeil, B., Schirnick, C., Steinfeldt, R., Suzuki, T., Tilbrook, B., Velo, A., Wanninkhof, R., and Woosley, R. J.: An updated version of the global interior ocean biogeochemical data product, GLODAPv2.2020, Earth Syst. Sci. Data, 12, 3653–3678, https://doi.org/10.5194/essd-12-3653-2020, 2020.

O'Mara, N. A., Cheung, A. H., Kelly, C. S., Sandwick, S., Herbert, T. D., Russell, J. M., Abella-Gutiérrez, J., Dee, S. G., Swarzenski, P. W., and Herguera, J. C.: Subtropical Pacific Ocean Temperature Fluctuations in the Common Era: Multidecadal Variability and Its Relationship With Southwestern North American Megadroughts, Geophys. Res. Lett., 46, 14662–14673, https://doi.org/10.1029/2019GL084828, 2019.

Osborne, E. B., Thunell, R. C., Gruber, N., Feely, R. A., and Benitez-Nelson, C. R.: Decadal variability in twentieth-century ocean acidification in the California Current Ecosystem, Nat. Geosci., 13, 43–49, https://doi.org/10.1038/s41561-019-0499-z, 2020.

Phleger, F. B. and Soutar, A.: Production of Benthic Foraminifera in Three East Pacific Oxygen Minima, Micropaleontology, 19, 110, https://doi.org/10.2307/1484973, 1973.

Quay, P., Sonnerup, R., Westby, T., Stutsman, J., and McNichol, A.: Changes in the $^{13}C/^{12}C$ of dissolved inorganic carbon in the ocean as a tracer of anthropogenic CO_2 uptake: Changes in the $^{13}C/^{12}C$ of DIC in the Ocean, Glob. Biogeochem. Cycles, 17, 4-1-4–20, https://doi.org/10.1029/2001GB001817, 2003.

Quay, P., Sonnerup, R., Munro, D., and Sweeney, C.: Anthropogenic CO_2 accumulation and uptake rates in the Pacific Ocean based on changes in the $^{13}C/^{12}C$ of dissolved inorganic carbon, Glob. Biogeochem. Cycles, 31, 59–80, https://doi.org/10.1002/2016GB005460, 2017.

Racapé, V., Pierre, C., Metzl, N., Lo Monaco, C., Reverdin, G., Olsen, A., Morin, P., Vázquez-Rodríguez, M., Ríos, A. F., and Pérez, F. F.: Anthropogenic carbon changes in the Irminger Basin (1981–2006): Coupling $\delta^{13}C_{DIC}$ and DIC observations, J. Mar. Syst., 126, 24–32, https://doi.org/10.1016/j.jmarsys.2012.12.005, 2013.

Ravelo, A. C. and Fairbanks, R. G.: Oxygen Isotopic Composition of Multiple Species of Planktonic Foraminifera: Recorders of the Modern Photic Zone Temperature Gradient, Paleoceanography, 7, 815–831, https://doi.org/10.1029/92PA02092, 1992.

Rubino, M., Etheridge, D. M., Thornton, D. P., Howden, R., Allison, C. E., Francey, R. J., Langenfelds, R. L., Steele, L. P., Trudinger, C. M., Spencer, D. A., Curran, M. A. J., Van Ommen, T. D., and Smith, A. M.: Revised records of atmospheric trace gases CO_2, CH_4, N_2O, and $\delta^{13}C$-CO_2 over the last 2000 years from Law Dome, Antarctica, Earth Syst. Sci. Data, 11, 473–492, https://doi.org/10.5194/essd-11-473-2019, 2019.

Sarmiento, J. L. and Gruber, N.: Sinks for Anthropogenic Carbon, Phys. Today, 55, 30–36, https://doi.org/10.1063/1.1510279, 2002.

Sautter, L. R. and Thunell, R. C.: Seasonal Variability in the $\delta^{18}O$ and $\delta^{13}C$ of Planktonic Foraminifera from an Upwelling Environment: Sediment Trap Results from the San Pedro Basin, Southern California Bight, Paleoceanography, 6, 307–334, https://doi.org/10.1029/91PA00385, 1991.

Sonnerup, R. E., Quay, P. D., McNichol, A. P., Bullister, J. L., Westby, T. A., and Anderson, H. L.: Reconstructing the oceanic ^{13}C Suess Effect, Glob. Biogeochem. Cycles, 13, 857–872, https://doi.org/10.1029/1999GB900027, 1999.

Soutar, A. and Isaacs, J. D.: Abundance of pelagic fish during the 19th and 20th centuries as recorded in anaerobic sediment off the Californias, Fish. Bull., 72, 257–273, 1974.

Spero, H. J., Bijma, J., Lea, D. W., and Bemis, B. E.: Effect of seawater carbonate concentration on foraminiferal carbon and oxygen isotopes, Nature, 390, 497–500, https://doi.org/10.1038/37333, 1997.

Spindler, M., Hemleben, C., Salomons, J. B., and Smit, L. P.: Feeding behavior of some planktonic foraminifers in laboratory cultures, J. Foraminifer. Res., 14, 237–249, https://doi.org/10.2113/gsjfr.14.4.237, 1984.

Stoll, H. M., Bolton, C., Jaggi, M., Martinez-Garcia, A., and Bernasconi, S. M.: Divergent estimates of Miocene to Pleistocene upper ocean temperatures in the South Atlantic Ocean from alkenone and coccolith clumped isotope proxies, Clim. Past, 21, 2189–2203, https://doi.org/10.5194/cp-21-2189-2025, 2025.

Sverdrup, H. U. and Allen, W. E.: Distribution of diatoms in relation to the character of water masses and currents off southern California in 1938, J. Mar. Res., 2, 131–144, 1939.

Tagliabue, A. and Bopp, L.: Towards understanding global variability in ocean carbon-13, Glob. Biogeochem. Cycles, 22, https://doi.org/10.1029/2007GB003037, 2008.

Tans, P.: Reminiscing on the Use and Abuse of ^{14}C and ^{13}C in Atmospheric CO_2, Radiocarbon, 64, 747–760, https://doi.org/10.1017/RDC.2022.7, 2022.

Thunell, R. C.: Seasonal and annual variability in particle fluxes in the Gulf of California: A response to climate forcing, Deep Sea Res. Part Oceanogr. Res. Pap., 45, 2059–2083, https://doi.org/10.1016/S0967-0637(98)00053-3, 1998.

Van Geen, A., McCorkle, D. C., and Klinkhammer, G. P.: Sensitivity of the phosphate-cadmium-carbon isotope relation in the ocean to cadmium removal by suboxic sediments, Paleoceanography, 10, 159–169, https://doi.org/10.1029/94PA03352, 1995.

Verwega, M.-T., Somes, C. J., Schartau, M., Tuerena, R. E., Lorrain, A., Oschlies, A., and Slawig, T.: Description of a global marine particulate organic carbon-13 isotope data set, Earth Syst. Sci. Data, 13, 4861–4880, https://doi.org/10.5194/essd-13-4861-2021, 2021.

Wanninkhof, R., Park, G.-H., Takahashi, T., Sweeney, C., Feely, R., Nojiri, Y., Gruber, N., Doney, S. C., McKinley, G. A., Lenton, A., Le Quéré, C., Heinze, C., Schwinger, J., Graven, H., and Khatiwala, S.: Global ocean carbon uptake: magnitude, variability and trends, Biogeosciences, 10, 1983–2000, https://doi.org/10.5194/bg-10-1983-2013, 2013.

Wefer, G. and Berger, W. H.: Isotope paleontology: growth and composition of extant calcareous species, Mar. Geol., 100, 207–248, https://doi.org/10.1016/0025-3227(91)90234-U, 1991.

Weiss, R. F.: Carbon dioxide in water and seawater: the solubility of a non-ideal gas, Mar. Chem., 2, 203–215, https://doi.org/10.1016/0304-4203(74)90015-2, 1974.

Wolfe, W. H., Martz, T. R., Dickson, A. G., Goericke, R., and Ohman, M. D.: A 37-year record of ocean acidification in the Southern California current, Commun. Earth Environ., 4, 406, https://doi.org/10.1038/s43247-023-01065-0, 2023.

623 Young, J. N., Bruggeman, J., Rickaby, R. E. M., Erez, J., and Conte, M.: Evidence for changes in carbon
624 isotopic fractionation by phytoplankton between 1960 and 2010: 50 Year Record of Global Surface ε_p,
625 Glob. Biogeochem. Cycles, 27, 505–515, https://doi.org/10.1002/gbc.20045, 2013.

626